JACS
JOURNAL OF THE AMERICAN CHEMICAL SOCIETY

Communication

pubs.acs.org/JACS

Unexpected Efficient Synthesis of Millimeter-Scale Single-Wall Carbon Nanotube Forests Using a Sputtered MgO Catalyst Underlayer Enabled by a Simple Treatment Process

Takashi Tsuji,[†,‡] Kenji Hata,[†,‡] Don N. Futaba,[*,†,‡] and Shunsuke Sakurai[*,†,‡]

[†]CNT-Application Research Center, National Institute of Advanced Industrial Science and Technology (AIST), Central 5, 1-1-1 Higashi, Tsukuba, Ibaraki 305-8565, Japan

[‡]Research Association for Single Wall Carbon Nanotubes (TASC), Central 5, 1-1-1 Higashi, Tsukuba, Ibaraki 305-8565, Japan

Supporting Information

ABSTRACT: An unexpected 5000% increase in growth efficiency and high (95%) single-wall selectivity synthesis of vertically aligned carbon nanotubes (CNTs) was shown from Fe catalysts supported on a sputtered MgO underlayer from a simple underlayer treatment, i.e., annealing treatment. In this way, millimeter-scale single-wall carbon nanotube "forests" could be synthesized in a 10 min time, which has never been previously reported for MgO catalyst underlayer or any underlayer besides Al_2O_3. This level of efficiency and characterized SWCNT properties were similar to those grown using Al_2O_3 underlayers. Spectroscopic and microscopic analyses revealed that the treatment improved stability of the catalyst nanoparticle array by the suppressing catalyst subsurface diffusion and retaining the metallic state of the surface Fe atoms. Taken together, these results reveal a new route in achieving highly efficient SWCNT synthesis.

Synthesis of single-wall carbon nanotubes (SWCNTs) remains a vital research topic in the effort to elucidate and utilize their properties since their discovery in 1993.[1,2] Over the subsequent 23 years, the synthesis of SWCNTs has seen great advancement in efficiency spanning laser ablation, arc discharge, and chemical vapor deposition (CVD) methods.[3−5] Increased synthesis efficiency affords longer and cleaner SWCNTs, which have proven to be advantageous for numerous applications spanning composite materials,[6] energy devices,[7,8] and sensors.[9] One of the most common methods to synthesize long SWCNTs is to grow them by CVD from catalyst nanoparticles supported on a substrate whereupon the SWCNTs self-assemble into a vertically aligned array, which is commonly referred to as a "forest", "carpet", or "array".[10−13] In addition to length, SWCNTs in these forests have shown to possess high purity and high specific surface area. Interestingly, despite the many advancements in synthesis, all reports of efficient (i.e., millimeter-scale) SWCNT synthesis require an Al_2O_3 catalyst underlayer[14−22] as the interaction between the catalyst and the underlayer is critical in supporting the formation of an array of small (c.a. ∼ 2−3 nm) and high density (∼15 nm spacing) nanoparticles, which is stable throughout the CVD process.[23−25]

Reports on the use of other underlayer species, e.g., SiO_2, MgO, ZrO_2, or TiN, have shown difficulty in achieving high yield (e.g., >100 μm) of SWCNT forest.[10,26−33] These difficulties originate from the inability of the underlayer to maintain the catalyst nanoparticle size and number density.[27,34] For example, several groups have reported the use of single-crystal MgO as the catalyst underlayer material and have demonstrated the growth of tall (∼2 mm), few-walled CNT forests; however, the synthesis of SWCNTs has been limited to sub-100 μm.[29−32] In addition, the synthesis of SWCNT forests using a sputtered MgO or SiO_2 underlayer has shown difficulties in surpassing a forest height of tens of micrometers.[10,28] Furthermore, reports of synthesis of CNT forests using catalysts deposited on conductive supports, such as TiN, TiSiN, AlSi, and $CoSi_2$ have been limited to few-walled CNTs.[33−36] Amama et al. reported the difficulty to synthesize CNTs, in general, from an Fe catalyst on deposited MgO, ZrO_2, and TiN underlayers due to faster rates of subsurface diffusion and increase in the nanoparticle size.[27] These examples exemplify the crucial role of the underlayer in supporting a stable catalyst nanoparticle array for efficient, i.e., millimeter-scale, SWCNT synthesis. Therefore, expanding our ability to efficiently synthesize SWCNTs with other underlayers is of scientific interest as it further advances our understanding of CNT synthesis on supported catalysts.

In this Communication, we report the unexpected efficient synthesis of millimeter-scale SWCNT forests from Fe catalyst supported on a sputtered MgO underlayer by a simple treatment process, consisting of an ambient annealing treatment to the MgO underlayer prior to the Fe catalyst deposition. In this way, the sputtered MgO underlayer supported the formation of a stable catalyst nanoparticle array suitable for highly efficient (1.2 mm within 10 min growth time) and highly selective (∼95%) SWCNT forest synthesis. Furthermore, the level of growth efficiency as characterized by the in situ growth kinetics was on par with those grown on Al_2O_3. Through spectroscopic and microscopic analyses, we interpret that the underlayer treatment increased crystallinity, that suppressed Fe subsurface diffusion and retained the Fe metallic state, which were essential for the improved nanoparticle stability and growth efficiency. These findings are surprising and suggest that highly efficient synthesis of SWCNTs can be expanded to various catalyst underlayers lacking sufficient crystallinity and advance our grasp of the deactivation mechanisms currently limiting SWCNT synthesis.

Received: October 26, 2016
Published: December 15, 2016

DOI: 10.1021/jacs.6b11189
J. Am. Chem. Soc. 2016, 138, 16608−16611

Catalyst MgO underlayers (110 nm) were prepared by magnetron sputtering on Si wafers with a 500 nm thermally grown oxide layer, followed by annealing treatment at 750 °C for 20 min in an air ambient. Then, Fe film (1.8 nm) was deposited onto the underlayer. For comparison, standard Al_2O_3/Fe (40 nm/1.8 nm) underlayer/catalyst were also prepared by sequential sputtering.

Nanoparticle formation was performed by introducing the substrate into preheated, 1 in. furnace (650 °C for MgO, 750 °C for Al_2O_3) and annealed for 6 min in H_2:He = 9:1 at ambient pressure to convert the Fe film into catalyst nanoparticles. Then, SWCNT forests were synthesized by water-assisted chemical vapor deposition process[11] with a C_2H_2 (0.4%) carbon feedstock, a H_2O (~200 ppm) growth enhancer, and He carrier gas (total flow of 1000 sccm at ambient pressure) at 750 °C with a growth time of 10 min.

To begin, we demonstrate the efficient synthesis of CNTs from a Fe catalyst on a sputtered MgO underlayer by applying a treatment to the MgO underlayer (Figure 1). To highlight the

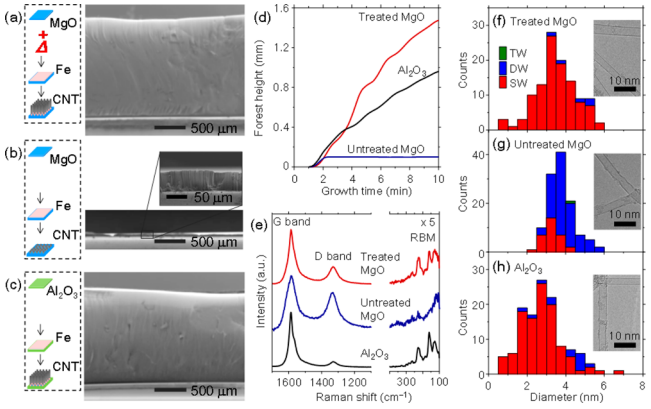

Figure 1. SEM images of the CNT forests grown using a (a) treated MgO, (b) untreated MgO, and (c) Al_2O_3 underlayer (insets: schematics for each process). (d) Growth kinetics curves of CNT forests grown using the treated MgO (red), untreated MgO (blue), and Al_2O_3 underlayers (black) (e) Raman spectra of CNT forests grown using the treated MgO (red), untreated MgO (blue), and Al_2O_3 underlayers (black). Histograms of the diameter and wall number distributions for (f) treated MgO, (g) untreated MgO, and (h) Al_2O_3 underlayers (insets: representative TEM images). SW, DW, and TW represent single wall, double wall, and triple wall CNTs, respectively.

effect, two separate Fe/MgO catalyst substrates were prepared with and without the MgO treatment prior to Fe deposition (denoted: "treated" and "untreated," respectively). When grown, the treated underlayer sample exhibited highly efficient synthesis of vertically aligned CNTs over one millimeter in a 10 min growth time (Figure 1a). These results represent an unexpected and >5000% enhancement in growth efficiency when compared to the nonuniform growth of CNTs (~20 μm) using the untreated case (Figure 1b). Furthermore, the yield achieved the level of that grown from Fe deposited on an Al_2O_3 underlayer, which is well-known to grow millimeter-scale SWCNT forests (Figure 1c). The forest growth kinetics curves (i.e., forest height vs time) for the three cases (Figure 1d) showed similar behavior: a high growth rate at the onset of growth followed by an exponential decrease until termination. However, a significant difference can be observed in the catalytic growth lifetime. In contrast to the untreated case which terminated within 1.5 min, synthesis using the treated MgO substrate exhibited an extended lifetime (>10 min) similar to the case of Al_2O_3. The SWCNT growth efficiency using this underlayer of treated sputtered MgO ranks among the highest reported, which exclusively use an Al_2O_3 underlayer.[14−22]

Significantly, the CNT forest synthesized using a treated sputtered MgO underlayer was found to possess a 95% SWCNT selectivity. The CNT forest was characterized by Raman spectroscopy and transmission electron microscopy (TEM) (Figure 1e−h). First, Raman (532 nm) for the treated case showed typical features of SWCNTs, such as the intensity ratio of the graphitic-to-disorder bands (G/D ratio) of ~4 and clear radial breathing mode (RBM) peaks (indicative of SWCNTs) at 129, 162, and 225 cm^{-1}, which were similar to SWCNTs grown using Al_2O_3 (Figure 1e). In contrast, the Raman spectrum for the untreated case showed a decreased G/D ratio (~2) and an absence of RBM peaks, which is more typical of multiwalled carbon nanotubes (MWCNTs) (Figure 1e). Second, TEM observations for the treated case showed high concentrations of SWCNTs, similar to that of Al_2O_3. A histogram of the diameter and wall number distribution (Figure 1f) showed that the CNTs for the treated case were 95% SWCNTs with a diameter of 3.5 ± 0.95 nm (HRTEM images are shown in the Supporting Information). Although this average diameter is large and the distribution is quite wide, these sizes are quite similar to SWCNTs grown in a forest using an Al_2O_3 underlayer. As shown in Figure 1h, the SWCNTs grown using Al_2O_3 show >90% SWCNT selectivity with an average diameter of 2.8 ± 0.97 nm. This large diameter is typical for SWCNTs grown in a forest by water-assisted CVD and has been found to be a necessary structural feature to enable highly efficient synthesis.[24] In contrast, the untreated case showed both increased presence of double-walled CNTs and diameter (ave.: 1.7 walls) and diameter (3.8 nm) (Figure 1g). Taken together, these results demonstrate an unexpected and unprecedented enhancement in SWCNT growth efficiency using a deposited MgO underlayer made possible by a simple treatment.

SWCNTs grown from the treated MgO case demonstrated a similar quality as those grown using an Al_2O_3 underlayer. We investigated the forest macroscopic properties which are known to be sensitive to the level of crystalline defects, purity, diameter, wall number, and alignment. As two metrics, we employed thermal diffusivity of the forest along the CNT axis and the electrical conductivity of the forest after densification into an aligned CNT sheet. Thermal diffusivity was measured by the flash method using a xenon lamp source (Netzsch, LFA 447 NanoFlash) and was estimated to be 50 mm^2/s for the CNT forest on treated MgO, which was slightly lower than that grown using Al_2O_3 (78 mm^2/s) but comparable with literature values (50−65 mm^2/s) (Figure 2a).[37−39] The electrical conductivity characterization was performed on aligned solid sheets prepared by liquid-induced collapse of the forests and measured by the four-probe method (LORESTRA-EP MCP-T360).[40] The electrical conductivity of the SWCNTs grown using the treated

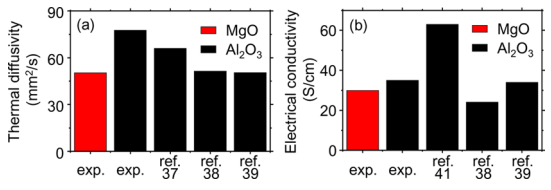

Figure 2. Graphs comparing the (a) thermal diffusivity and (b) electrical conductivity, respectively, of CNTs grown using the treated MgO (red) and Al_2O_3 (black), as grown in this report and found in the literature.

DOI: 10.1021/jacs.6b11189
J. Am. Chem. Soc. 2016, 138, 16608−16611

MgO (30 S/cm) was found to be comparable with that grown using Al_2O_3 (35 S/cm) as prepared in this study and in the literature (25−63 S/cm) (Figure 2b).[38,39,41] The similarity in the thermal diffusivity and electrical conductivity indicates the comparable quality of the SWCNTs grown by the treated MgO case and those grown using Al_2O_3.

To gain deeper understanding of the increased growth efficiency and SWCNT selectivity, we performed elemental depth-profiling analysis of the catalyst/underlayer surface by X-ray photoelectron spectroscopy (XPS). Depth profiling was carried out by Ar^+ etching (2.0 kV) at a rate of 2.2 nm/min estimated from the required time to remove the entire MgO (110 nm) layer. An ex situ XPS analysis (Quantera SXM X-ray photoelectron spectrometer (Al 1486.6 eV)) was carried out on both the treated and untreated samples after 5 min exposure to the ambient (He, 750 °C) following nanoparticle formation (Figure 3a−d). The Fe atomic concentration was estimated from

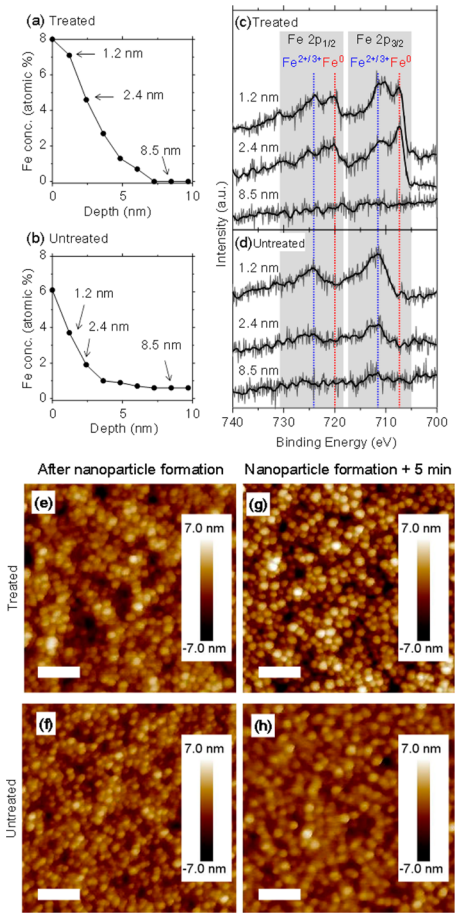

Figure 3. XPS depth profiles for the (a) treated and (b) untreated cases. Individual XPS Fe 2p profiles (gray, raw spectra; black, smoothed spectra obtained by Savitzky−Golay method) at different depths for the (c) treated and (d) untreated cases. (e−h) AFM images of the treated and untreated cases before and after additional 5 min exposure to the ambient (Scale bars: 50 nm).

the areas of the Fe $2p_{3/2}$, Mg 2p, and O 1s XPS peaks. XPS depth-profiling revealed that the profiles for both the treated and untreated cases were characterized by a nonlinear decrease in Fe concentration with the highest concentration located at the surface. For the treated case, the surface concentration of Fe was ∼8% and following the nonlinear decrease, the Fe concentration became almost zero at a depth of 7.5−8.5 nm. The untreated case depth profile exhibited several differences. First, the concentration at the surface was lower (∼6%). Second, the nonlinear decrease in Fe concentration extended far deeper into the underlayer and detectable a depth beyond 8.5 nm (Figure 3a,b). In addition, comparison of individual spectra taken at different depths revealed a significant difference in the surface Fe oxidation state. Specifically, from the presence of the Fe^0 state in the Fe $2p_{3/2}$ (707 eV) and Fe $2p_{1/2}$ (720 eV) peaks of the treated case, metallic Fe was present near the surface (Figure 3c). In contrast, Fe^0 state was not observed for the untreated case (Figure 3d). These results clearly show that the underlayer treatment not only reduces the rate of Fe subsurface diffusion,[23,42] but aids in retaining the metallic state of the surface Fe.

Topographic analysis of the catalytic surface was performed at two stages by ex situ AFM immediately following the nanoparticle formation and after an additional 5 min exposure to the ambient (He, 750 °C) (Bruker Dimension V, FastScan). Interestingly, for both the treated and untreated cases, immediately following the nanoparticle formation, the estimated nanoparticle number densities and sizes were nearly identical at 5.8×10^{11} cm^{-2} and 3−4 nm, respectively, (Figure 3e,f) which is typical for SWCNT forests.[43] However, after an additional 5 min exposure to the ambient, the treated case showed no significant change in both nanoparticle number density (5.8×10^{11} cm^{-2} to 6.2×10^{11} cm^{-2}) and size, whereas the untreated case exhibited a 50% decrease in number density (5.8×10^{11} cm^{-2} to 3.0×10^{11} cm^{-2}) and slight increase in particle size to ∼4 nm (Figure 3g,h). The AFM results are in agreement with the XPS observation that the treated case was less affected by subsurface diffusion and further indicate that Fe surface migration[15,44] does not occur significantly fast, affording stable nanoparticle number density and size. Taken together, these results provide clear evidence of the increased stability of the Fe nanoparticle array density by the underlayer treatment.

We interpret that the improved catalyst stability results from increased crystallinity as reported through the sintering of MgO thin film in an air ambient.[45] The increased crystallinity reduces Fe diffusion pathways (e.g., vacancies, grain boundaries, etc.), present in the as-deposited underlayer, which inhibits Fe subsurface diffusion to create a stable nanoparticle array as observed experimentally. While the stability in the nanoparticle size and density are both essential for SWCNT synthesis efficiency, our experimental results further indicate that the electronic state of the Fe catalyst nanoparticles is also essential. In addition, the absence of metallic Fe in the untreated case suggest that the nanoparticles observed by AFM are not active catalysts, and do not contribute to synthesis. This would also explain why we do not observe a larger change in nanoparticle size after prolonged exposure to the ambient by topographic analysis using AFM (Figure 3h). Thus, the existence of surface metallic Fe indicates the presence of Fe catalyst nanoparticles, and the underlayer treatment affords the retention of the surface metallic Fe in the form of a catalyst nanoparticle array resulting in high efficiency SWCNT synthesis. We postulate that the treatment can be applied to other underlayer systems possessing insufficient crystallinity for the CNT synthesis.

In conclusion, we demonstrate the unexpected highly efficient synthesis of millimeter-scale SWCNT forest from Fe catalysts on a sputtered MgO underlayer by a simple underlayer treatment. Elemental and topographic analysis of the surface revealed that the treatment improved stability of the catalyst nanoparticle array by inhibiting catalyst subsurface diffusion and retaining the

DOI: 10.1021/jacs.6b11189
J. Am. Chem. Soc. 2016, 138, 16608−16611

metallic state of the surface Fe. Our analyses suggest that these aspects brought about by the underlayer treatment explain the 5000% improvement in growth efficiency. We postulate that this approach is not limited to MgO; therefore, these findings provide a more general understanding of carbon nanotube synthesis for supported catalysts. We hope that this work invokes further research on the treatment of the catalyst underlayer as we believe that this technique has yet to be fully understood and optimized.

■ ASSOCIATED CONTENT

Supporting Information

The Supporting Information is available free of charge on the ACS Publications website at DOI: 10.1021/jacs.6b11189.

HRTEM images of SWCNTs grown using a treated MgO (PDF)

■ AUTHOR INFORMATION

Corresponding Authors

*S.S. shunsuke-sakurai@aist.go.jp
*D.N.F. d-futaba@aist.go.jp

ORCID

Shunsuke Sakurai: 0000-0002-0465-3274

Notes

The authors declare no competing financial interest.

■ ACKNOWLEDGMENTS

This paper is based on results obtained from a project commissioned by the New Energy and Industrial Technology Development Organization (NEDO).

■ REFERENCES

(1) Iijima, S.; Ichihashi, T. *Nature* **1993**, *363*, 603.
(2) Bethune, D. S.; Klang, C. H.; de Vries, M. S.; Gorman, G.; Savoy, R.; Vazquez, J.; Beyers, R. *Nature* **1993**, *363*, 605.
(3) Thess, A.; Lee, R.; Nikolaev, P.; Dai, H.; Petit, P.; Robert, J.; Xu, C.; Lee, Y. H.; Kim, S. G.; Rinzler, A. G.; Colbert, D. T.; Scuseria, G. E.; Tomanek, D.; Fischer, J. E.; Smalley, R. E. *Science* **1996**, *273*, 483.
(4) Journet, C.; Maser, W. K.; Bernier, P.; Loiseau, A.; Lamy de la Chapelle, M.; Lefrant, S.; Deniard, P.; Lee, R.; Fischer, J. E. *Nature* **1997**, *388*, 756.
(5) Nikolaev, P.; Bronikowski, M. J.; Bradley, R. K.; Rohmund, F.; Colbert, D. T.; Smith, K. A.; Smalley, R. E. *Chem. Phys. Lett.* **1999**, *313*, 91.
(6) Sekitani, T.; Noguchi, Y.; Hata, K.; Fukushima, T.; Aida, T.; Someya, T. *Science* **2008**, *321*, 1468.
(7) Liu, B.; Soares, P.; Checkles, C.; Zhao, Y.; Yu, G. *Nano Lett.* **2013**, *13*, 3414.
(8) Laszczyk, K. U.; Kobashi, K.; Sakurai, S.; Sekiguchi, A.; Futaba, D. N.; Yamada, T.; Hata, K. *Adv. Energy Mater.* **2015**, *5*, 1500741.
(9) Snow, E. S.; Perkins, F. K.; Houser, E. J.; Badescu, S. C.; Reinecke, T. L. *Science* **2005**, *307*, 1942.
(10) Murakami, Y.; Chiashi, S.; Miyauchi, Y.; Hu, M.; Ogura, M.; Okubo, T.; Maruyama, S. *Chem. Phys. Lett.* **2004**, *385*, 298.
(11) Hata, K.; Futaba, D. N.; Mizuno, K.; Namai, T.; Yumura, M.; Iijima, S. *Science* **2004**, *306*, 1362.
(12) Xu, Y.-Q.; Flor, E.; Kim, M. J.; Hamadani, B.; Schmidt, H.; Smalley, R. E.; Hauge, R. H. *J. Am. Chem. Soc.* **2006**, *128*, 6560.
(13) Pint, C. L.; Xu, Y. Q.; Pasquali, M.; Hauge, R. H. *ACS Nano* **2008**, *2*, 1871.
(14) Noda, S.; Hasegawa, K.; Sugime, H.; Kakehi, K.; Zhang, Z.; Maruyama, S.; Yamaguchi, Y. *Jpn. J. Appl. Phys.* **2007**, *46*, L399.
(15) Amama, P. B.; Pint, C. L.; McJilton, L.; Kim, S. M.; Stach, E. A.; Murray, P. T.; Hauge, R. H.; Maruyama, B. *Nano Lett.* **2009**, *9*, 44.
(16) Chakrabarti, S.; Kume, H.; Pan, L.; Nagasaka, T.; Nakayama, Y. *J. Phys. Chem. C* **2007**, *111*, 1929.
(17) Xu, Y.-Q.; Flor, E.; Schmidt, H.; Smalley, R. E.; Hauge, R. H. *Appl. Phys. Lett.* **2006**, *89*, 123116.
(18) Zhong, G.; Hofmann, S.; Yan, F.; Telg, H.; Warner, J. H.; Eder, D.; Thomsen, C.; Milne, W. I.; Robertson, J. *J. Phys. Chem. C* **2009**, *113*, 17321.
(19) Islam, A. E.; Nikolaev, P.; Amama, P. B.; Saber, S.; Zakharov, D.; Huffman, D.; Erford, M.; Sargent, G.; Semiatin, S. L.; Stach, E. A.; Maruyama, B. *Nano Lett.* **2014**, *14*, 4997.
(20) Youn, S. K.; Yazdani, N.; Patscheider, J.; Park, H. G. *RSC Adv.* **2013**, *3*, 1434.
(21) Han, Z. J.; Ostrikov, K. *J. Am. Chem. Soc.* **2012**, *134*, 6018.
(22) Zhong, G.; Iwasaki, T.; Robertson, J.; Kawarada, H. *J. Phys. Chem. B* **2007**, *111*, 1907.
(23) Amama, P. B.; Pint, C. L.; Kim, S. M.; McJilton, L.; Eyink, K. G.; Stach, E. A.; Hauge, R. H.; Maruyama, B. *ACS Nano* **2010**, *4*, 895.
(24) Chen, G.; Davis, R. C.; Futaba, D. N.; Sakurai, S.; Kobashi, K.; Yumura, M.; Hata, K. *Nanoscale* **2016**, *8*, 162.
(25) Mattevi, C.; Wirth, C. T.; Hofmann, S.; Blume, R.; Cantoro, M.; Ducati, C.; Cepek, C.; Knop-gericke, A.; Milne, S.; Castellarin-cudia, C.; Dolafi, S.; Goldoni, A.; Schloegl, R.; Robertson, J. *J. Phys. Chem. C* **2008**, *112*, 12207.
(26) Zhang, G.; Mann, D.; Zhang, L.; Javey, A.; Li, Y.; Yenilmez, E.; Wang, Q.; McVittie, J. P.; Nishi, Y.; Gibbons, J.; Dai, H. *Proc. Natl. Acad. Sci. U. S. A.* **2005**, *102*, 16141.
(27) Amama, P. B.; Pint, C. L.; Mirri, F.; Pasquali, M.; Hauge, R. H.; Maruyama, B. *Carbon* **2012**, *50*, 2396.
(28) Lee, T. J.; Seo, J.; Lee, H. *J. Korean Phys. Soc.* **2008**, *53*, 3236.
(29) Pint, C.; Pheasant, S.; Nicholas, N.; Horton, C.; Hauge, R. *J. Nanosci. Nanotechnol.* **2008**, *8*, 6158.
(30) He, M.; Vasala, S.; Jiang, H.; Karppinen, M.; Kauppinen, E. I.; Niemelä, M.; Lehtonen, J. *Carbon* **2012**, *50*, 4750.
(31) Xiong, G.-Y.; Wang, D. Z.; Ren, Z. F. *Carbon* **2006**, *44*, 969.
(32) Ohashi, T.; Shima, T. *Carbon* **2015**, *87*, 453.
(33) Yang, J.; Esconjauregui, S.; Sugime, H.; Makaryan, T.; Hallam, T.; Duesberg, G. S.; Robertson, J. *Phys. Status Solidi B* **2014**, *251*, 2389.
(34) Yang, J.; Esconjauregui, S.; Robertson, A. W.; Guo, Y.; Hallam, T.; Sugime, H.; Zhong, G.; Duesberg, G. S.; Robertson, J. *Appl. Phys. Lett.* **2015**, *106*, 083108.
(35) Esconjauregui, S.; Bayer, B. C.; Fouquet, M.; Wirth, C. T.; Yan, F.; Xie, R.; Ducati, C.; Baehtz, C.; Castellarin-Cudia, C.; Bhardwaj, S.; Cepek, C.; Hofmann, S.; Robertson, J. *J. Appl. Phys.* **2011**, *109*, 114312.
(36) Bayer, B. C.; Zhang, C.; Blume, R.; Yan, F.; Fouquet, M.; Wirth, C. T.; Weatherup, R. S.; Lin, L.; Baehtz, C.; Oliver, R. A.; Knop-Gericke, A.; Schlögl, R.; Hofmann, S.; Robertson, J. *J. Appl. Phys.* **2011**, *109*, 114314.
(37) Akoshima, M.; Hata, K.; Futaba, D. N.; Mizuno, K.; Baba, T.; Yumura, M. *Jpn. J. Appl. Phys.* **2009**, *48*, 05EC07.
(38) Matsumoto, N.; Oshima, A.; Chen, G.; Yudasaka, M.; Yumura, M.; Hata, K.; Futaba, D. N. *Carbon* **2015**, *87*, 239.
(39) Matsumoto, N.; Chen, G.; Yumura, M.; Futaba, D. N.; Hata, K. *Nanoscale* **2015**, *7*, 5126.
(40) Futaba, D. N.; Hata, K.; Yamada, T.; Hiraoka, T.; Hayamizu, Y.; Kakudate, Y.; Tanaike, O.; Hatori, H.; Yumura, M.; Iijima, S. *Nat. Mater.* **2006**, *5*, 987.
(41) Chen, G.; Futaba, D. N.; Sakurai, S.; Yumura, M.; Hata, K. *Carbon* **2014**, *67*, 318.
(42) Kim, S. M.; Pint, C. L.; Amama, P. B.; Zakharov, D. N.; Hauge, R. H.; Maruyama, B.; Stach, E. A. *J. Phys. Chem. Lett.* **2010**, *1*, 918.
(43) Futaba, D. N.; Hata, K.; Namai, T.; Yamada, T.; Mizuno, K.; Hayamizu, Y.; Yumura, M.; Iijima, S. *J. Phys. Chem. B* **2006**, *110*, 8035.
(44) Nessim, G. D.; Hart, A. J.; Kim, J. S.; Acquaviva, D.; Oh, J.; Morgan, C. D.; Seita, M.; Leib, J. S.; Thompson, C. V. *Nano Lett.* **2008**, *8*, 3587.
(45) Cáceres, D.; Vergara, I.; González, R. *J. Appl. Phys.* **2003**, *93*, 4300.

DOI: 10.1021/jacs.6b11189
J. Am. Chem. Soc. 2016, 138, 16608−16611